Supplementary material
"Why a falling drop does not in general behave like a rising bubble"

Manoj Kumar Tripathi, Kirti Chandra Sahu and and Rama Govindarajan[†]
Department of Chemical Engineering, Indian Institute of Technology Hyderabad, Yeddumailaram 502 205, Andhra Pradesh, India,
[†] *TIFR Centre for Interdisciplinary Sciences, Tata Institute of Fundamental Research, Narsingi, Hyderabad 500075, India.*
(Dated: March 10, 2014)

We describe the details of the numerical approach and the validation of our numerical algorithm in this supplementary material.

Numerical approach

A finite-volume approach in the diffuse-interface framework is incorporated to solve the system of equations (1), (5) and (6) of the main text, which are discretized on a staggered grid. The scalar variables (the pressure and the volume fraction of the outer fluid) and the velocity components are defined at the cell-centres and at the cell faces, respectively. A weighted-essentially-non-oscillatory (WENO) scheme is used for discretization of the advective term in Eq. (6), and a central difference scheme is used to discretize the diffusive term. In order to achieve second-order accuracy in the temporal discretization, the Adams-Bashforth and the Crank-Nicholson methods are used for the advective and second-order dissipation terms in Eq. (5), respectively. We assume the flow to be axisymmetric about the axis $x = 0$, and the Neumann boundary conditions are used at the rest of the boundaries which are kept sufficiently far away from the bubble/drop as mentioned in the main manuscript.

Some of the results in the present paper are for bubbles with density and viscosity about 3 orders of magnitude less than that of the surrounding fluid. This regime is tough to simulate and generally generates spurious currents due to wrong calculation of surface tension at the interface. Thus the open-source finite-volume fluid flow solver, Gerris created by Popinet [13] was used for the validation of our code. Gerris minimizes problem of spurious currents by using the balanced-force continuum surface force formulation for the calculation of surface tension. In Gerris, a volume of fluid (VOF) formulation has been used to track the interface, wherein the piecewise linear interface reconstruction is used for the volume fraction c to rebuild the interface, which remains thin in the prescribed limit for all the times. This code also allows for dynamic adaptive grid refinement at the interface separating the fluids. The details of the implementation can be found in the papers by Popinet [13, 14].

As mentioned in the main manuscript, apart from Gerris, recent developments in the field of lattice Boltzmann simulations [8, 9] allow one to simulate multiphase flows with high density ratios (of 500 or more) by using a clever doubly-attractive pseudo-potential. A high surface tension can be obtained here by defining this force from the superposition of two simultaneously attractive and repulsive potentials. This approach can hence accommodate high density ratios. Although, this method has not been used in the present study, we would like to mention that this approach may give computational advantages over classical flow solvers.

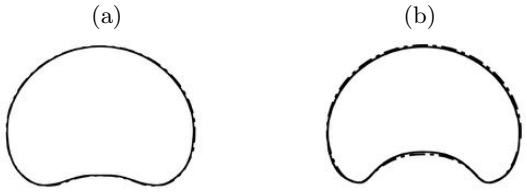

FIG. 1: Effect of domain size on the bubble shape at (a) $t = 4$, and (b) $t = 7$ for Ga = 3.09442, Bo = 29, $r = 7.4734 \times 10^{-4}$ and $m = 8.1536 \times 10^{-6}$. The solid and dot-dashed lines correspond to computational domains 8×24 and 16×48, respectively. The results are generated using square grid of $\Delta x = \Delta z = 0.015$.

We checked our simulations for different domain sizes and found that increasing domain size beyond 16×48 has no significant effect on the flow for $Re > 2$ (see for example Figure 1, which has been generated for Ga = 3.09442, Bo = 29, $r = 7.4734 \times 10^{-4}$ and $m = 8.1536 \times 10^{-6}$ at two time instants). The Reynolds number defined using the terminal velocity in this case is $Re \approx 1.8$. It is to be noted here that larger computational domains are required to study the flow dynamics for smaller Re, and care has been taken to provide results which are independent of domain size. For very low Re (figure 2 in the main paper), a computational domain of size 40×80 was used with Gerris [13]

with adaptive grid refinement, which reduced the computation time considerably (by about 4 times). The shape of

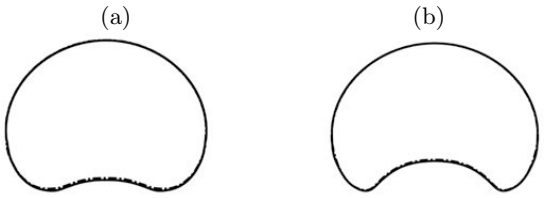

FIG. 2: Effect of grid refinement on the shape of the bubble at (a) $t = 4$, and (b) $t = 7$. The solid and dot-dashed lines correspond the results obtained using $\Delta x = \Delta z = 0.015$ and 0.0133, respectively. The rest of the parameter values are the same as those used in Figure 1.

the bubble at $t = 4$ and 7 for two different grids ($\Delta x = \Delta z = 0.02$ and 0.0133) in a computational domain of size 16×48 are shown in Figure 2. It is found that a square grid with $\Delta x = \Delta z = 0.015$ is enough to get results to within 0.1% accuracy.

Validation

Comparison with numerical simulations of Sussman & Smereka [5]

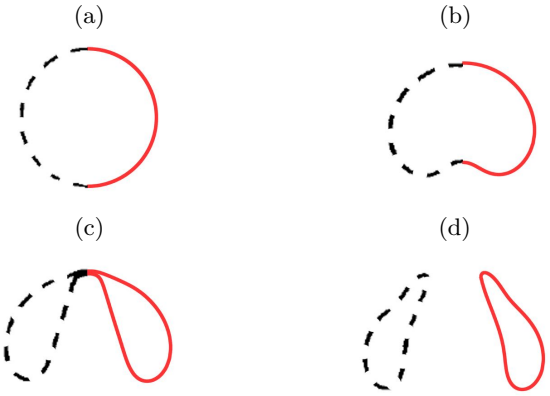

FIG. 3: Comparison of the shape of the bubble obtained from our simulation (shown by red line) with Sussman & Smereka [5] (dashed line) at various times: (a) $t = 0$, (b) $t = 0.8$, (c) $t = 1.6$ and (d) $t = 2.4$. The parameter values are Ga = 100, Bo = 200, $r = 0.001$ and $m = 0.01$.

In order to validate our code, in Figure 3 we compare our results obtained for Ga = 100, Bo = 200, $r = 0.001$ and $m = 0.01$ with those of Sussman & Smereka [5], who studied the fluid dynamics of rising bubble with topology change in the framework of a level-set approach. The dashed lines on the left hand side of each panel are the results from Sussman & Smereka [5], whereas the present results are plotted by solid red lines on the right hand side of the panels. It can be seen that the topology changes observed in our simulation agree excellently with the results of Sussman & Smereka [5].

Comparison with the experimental result of Bhaga & Weber [2]

In Figure 4, we compare the shape of the bubble obtained from our simulation (shown by the red line) with the corresponding results given in the experiment of Bhaga & Weber [2] (shown by the gray scale picture). The parameter values used to generate this figure are Ga = 3.09442, Bo = 29, $r = 7.4734 \times 10^{-4}$ and $m = 8.1536 \times 10^{-6}$, which are the values at which the experimental shape is presented in [2], after suitable transformation, as follows:

$$\mathrm{Ga} = \left(\frac{\mathrm{Bo}_{BW}^3}{64 Mo_{BW}} \right)^{\frac{1}{4}}, \quad \text{and} \quad \mathrm{Bo} = \frac{\mathrm{Bo}_{BW}}{4}, \tag{1}$$

where $Mo_{BW} = g\mu_o^4/\rho_o\sigma^3$, $Bo_{BW} = 4gR^2\rho_o/\sigma$, where the subscript BW refers to Bhaga & Weber. It can be seen that the shape of the bubble obtained from our numerical simulation is in qualitative agreement with the experimentally obtained drop of [2]. Note that a dimple at the bottom of the bubble (if one exists) in the experiment will not be visible in this photograph, and would appear just a horizontal edge at the bottom.

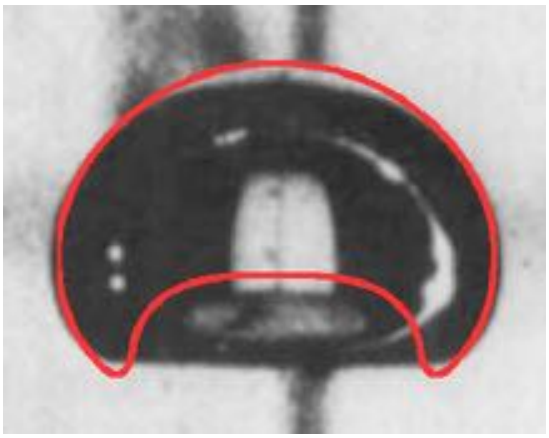

FIG. 4: Comparison of the shape of the bubble obtained from the present diffuse interface simulation (shown by red line) with that of Bhaga and Weber [2]. The parameter values are Ga = 3.09442, $Bo = 29$, $r = 7.4734 \times 10^{-4}$ and $m = 8.1536 \times 10^{-6}$.

Comparison with Han & Tryggvason [6]

The simulation domain was taken to be the same as that of Han & Tryggvason [6], i.e. 10×30 and the grid size was taken to be $\Delta x = \Delta z = 0.015$ for the parameter values stated in figure 5. The dimensionless time at which the drop breaks up ($t_{br} \approx 25.0$) is in agreement with the that of [6]. The oscillations in velocity are well replicated too.

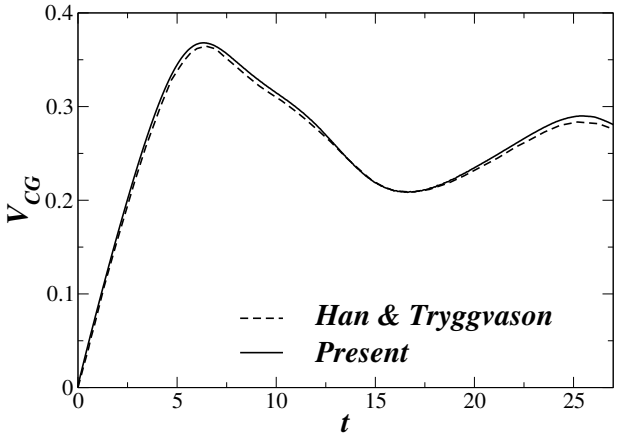

FIG. 5: Variation of velocity of center of gravity of the drop with time for $Ga = 219.09$, Bo = 240, $r = 1.15$ and $m = 1.1506$. The dashed line is the result due to Han & Tryggvason [6] and the solid line is the present result. The figure is plotted till breakup.

Comparison with analytical results

The next two comparisons are not so much for validation, since the analytical results are for idealised limits, but a demonstration that the analytical results are valid in a range of parameters lying near the idealized limits.

Cases	Joseph [1]	Present work
a	0.864	0.883
b	0.882	0.906

TABLE I: Comparison of the terminal velocities by Joseph [1] and the present work for the parameter values: (a) Ga = 50, and (b) Ga = 100. The rest of the parameter values are Bo = 10, $r = 0.001$ and $m = 0.01$.

In the Hadamard [3] limit

By balancing the drag force with the weight of the bubble/drop, and neglecting the inertial and surface tension forces, Rybczinsky [4] and Hadamard [3] analytically derived an expression for terminal velocity (famously known as Hadamard-Rybczinsky equation), which is given by

$$V_t = \frac{2}{3}\frac{R^2 g(r-1)\rho_1}{\mu_1}\left(\frac{1+m}{2+3m}\right). \tag{2}$$

Thus the dimensionless terminal velocity can be written as:

$$\widetilde{V_t} = \frac{2\mathrm{Ga}(1-r)}{3}\left(\frac{1+m}{2+3m}\right). \tag{3}$$

In an example simulation with the parameters Ga = 0.1, Bo = 0.1, $r = 0.001$ and $m = 0.01$, we found that the terminal velocity is $V_t = 0.0328$ for a domain of size 16×48 and larger. The corresponding dimensionless velocity obtained using equation (3) is 0.0333. In Figure 6 (a) and (b), we plot streamlines obtained from the Hadamard solution and our numerical simulations for Ga = 0.1. The qualitative similarity is apparent. The small discrepancies may be attributed to the fact that at $Re \to 0$ an infinitely large computational domain is required for accurate solutions, and also to small deviations from a spherical shape at our finite surface tension values, whereas the analytical result assumes a perfectly spherical bubble.

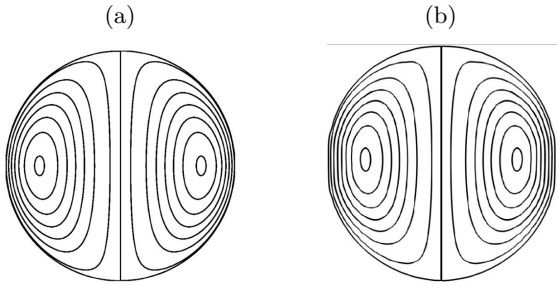

FIG. 6: Streamlines obtained from (a) the analytical result for Hadamard flow ($Re \to 0$) in a spherical bubble, and (b) the present simulation.

Comparison with potential flow solution

In Table I we compare the terminal velocities obtained from our numerical simulations for Ga = 50 and 100 with those obtained from the analytical solution of [1], who studied a rising spherical cap bubble in the potential flow regime. The other parameter values are Bo = 10, $r = 0.001$ and $m = 0.01$. In this parameter range, the computationally obtained bubble resembles a spherical cap. It can be seen that the potential flow assumption is able to predict the terminal velocity qualitatively.

The residual vorticity

A detailed discussion of what is the best way to estimate rotation within a drop is available in [11]. In axisymmetric flow the velocity-gradient tensor may be spilt into a symmetric part and an anti-symmetric part. The anti-symmetric part is the vorticity, of magnitude ω, oriented azimuthally. The eigenvalues of the symmetric part are given by $\pm s/2$,

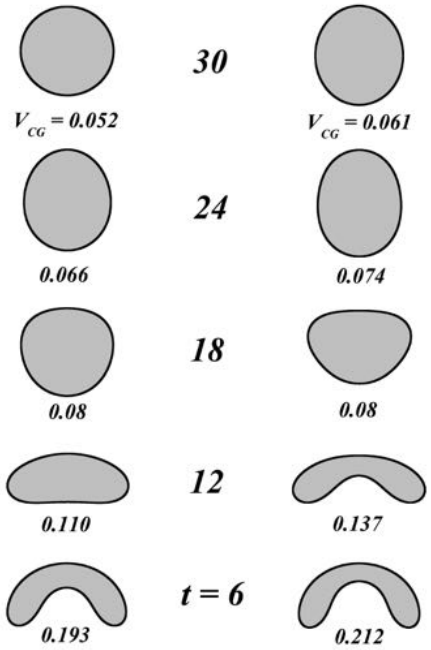

FIG. 7: (a) Evolution of bubble shape with time for $r = 0.9$, $m = 0.5$, $Re = 50$, $Bo = 50$, (b) evolution of drop shape with time for $r = 1.125$, $m = 0.625$, $Re = 50$, $Bo = 50$. The initial shape of both drop and bubble was kept spherical and the initial velocity given to the fluid blobs is $U_0 = 1$ for both.

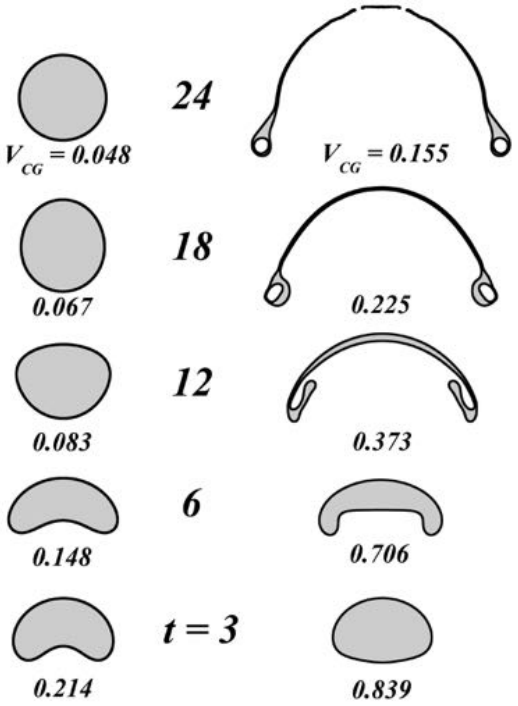

FIG. 8: (a) Evolution of bubble shape with time for $r = 0.52$, $m = 0.05$, $Re = 50$, $Bo = 50$, (b) evolution of drop shape with time for $r = 13$, $m = 1.25$, $Re = 50$, $Bo = 50$. The drop breaks up in the bag-breakup mode. The initial shape of both drop and bubble was kept spherical and the same initial velocity U_0 given to both fluid blobs.

where $s = (4u^2 + (u + w)^2)^{1/2}$. The vorticity in turn must can be decomposed into shear part and a pure rotational part. The latter is termed the residual vorticity, defined [10] as

$$\begin{aligned} \omega_{res} &= 0 \text{ for } |s| > |\omega| \\ &= sgn(\omega)(|\omega| - |s|) \text{ for } |s| \leq |\omega| \end{aligned} \tag{4}$$

where $sgn(\omega)$ is the signum function. The more standard Okubo-Weiss parameter

$$W = s_n^2 + s_s^2 - \omega^2, \tag{5}$$

wherein $s_n (\equiv \partial_x u - \partial_z w)$ and $s_s (\equiv \partial_x w - \partial_z u)$ are the normal and the shear components of the strain rate tensor respectively, is another measure of rotation in the flow. Both measures give similar images of the vortex cores in our simulations, but since the residual vorticity takes care to remove the shear part of the vorticity, we present results using this quantity.

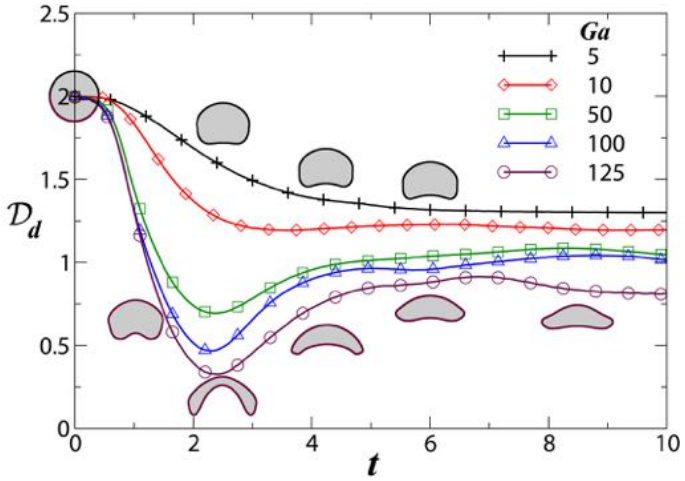

FIG. 9: Variation of dimple distance versus time for $Bo = 8$, $r = 7.4734 \times 10^{-4}$, $m = 8.5136 \times 10^{-6}$.

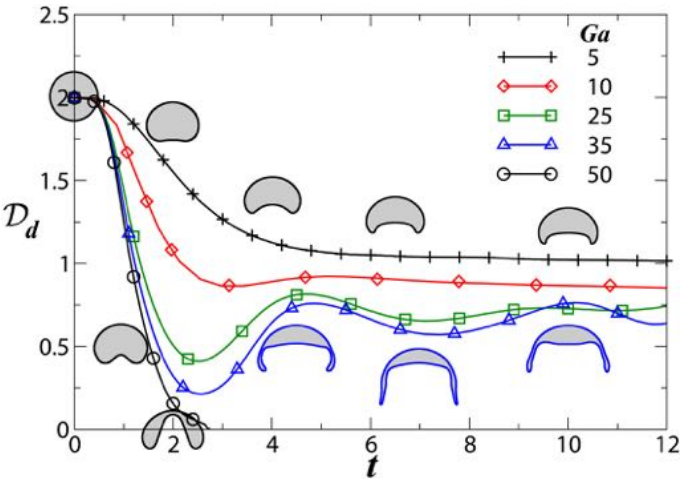

FIG. 10: Variation of dimple distance D_d versus time for $Bo = 29$, $r = 7.4734 \times 10^{-4}$, $m = 8.5136 \times 10^{-6}$.

Dynamics in zero-gravity

To study dynamics in zero gravity, we replace the Gallilei number by a Reynolds number $Re \equiv U_0 R/\nu$ based on the initial drop velocity U_0. Figure 7 shows a bubble and drop whose densities are close to that of the surrounding

fluid, and these evolve in a manner similar to each other. For a density ratio far from unity however, figure 8 gives an example where the drop breaks up in a bag-breakup mode while the bubble oscillates for some time but ultimately attains an equilibrium spherical shape.

Effects of viscosity

In this section we study the effects of viscosity on the tendency to break-up. That decreasing external fluid viscosity (increasing Gallilei number) will increase the tendency to break-up is demonstrated in figures 9 and 10 for two Bond numbers. Also oscillations become more prominent at higher Ga. If the viscosity ratio is low enough, the outer fluid is able to shear-break the drop. It is already known (see [12]) that a higher Weber number is required to break a drop when the surrounding fluid is more viscous. This indicates that the more the viscous drag, i.e. the less the inertia of the blob, the less willing it is to break. If the surrounding fluid is more viscous, we would need to increase gravity or reduce surface tension to break a blob. Thus, in effect, a higher Bond number is needed to break a blob. Figure 10 shows that when all the physical properties are kept the same while the kinematic viscosities are reduced in the same proportions for inner and outer fluids, the bubble tends to break up.

[1] Joseph, D. D. Rise velocity of a spherical cap bubble. *J. Fluid Mech.* **488**, 213–223 (2003).

[2] Bhaga, D. & Weber, M. E. Bubbles in viscous liquids: shapes, wakes and velocities. *J. Fluid Mech.* **105**, 61–85 (1981).

[3] Hadamard, J. Mouvement permanent lent dune sphere liquide et visqueuse dans un liquide visqueux. *CR Acad. Sci* **152**, 1735–1738 (1911).

[4] Rybzynski, W. ber die fortschreitende bewegung einer flssigen kugel in einem zhen medium. *Bull. Acad. Sci.* (1911).

[5] Sussman, M. & Smereka, P. Axisymmetric free boundary problems. *Journal of Fluid Mechanics* **341**, 269–294 (1997).

[6] Han, J. & Tryggvason, G. Secondary breakup of axisymmetric liquid drops. i. acceleration by a constant body force. *Physics of fluids* **11**, 3650 (1999).

[7] Popinet, S. Gerris: a tree-based adaptive solver for the incompressible euler equations in complex geometries. *Journal of Computational Physics* **190**, 572–600 (2003).

[8] Falcucci, G. & Ubertini, S. & Succi, S. Lattice Boltzmann simulations of phase-separating flows at large density ratios: the case of doubly-attractive pseudo-potentials. *Soft Matter* **6**, 43574365 (2010).

[9] Sbragaglia, M., Benzi, R., Biferale, L. , Succi, S., Sugiyama, K.& Toschi, F. Generalized lattice Boltzmann method with multirange pseudopotential. *Phys. Rev. E* **75**, 026702 (2007).

[10] Kolář, V. 2d velocity-field analysis using triple decomposition of motion. In *Proceedings of the 15th Australasian Fluid Mechanics Conference, CD-ROM, Paper AFMC00017<http://www. aeromech. usyd. edu. au/15afmc>, University of Sydney, Sydney, Australia* (2004).

[11] Thampi, S. P., Adhikari, R. & Govindarajan, R. Do liquid drops roll or slide on inclined surfaces?. *Langmuir* **29**, 3339–3346 (2013).

[12] Cohen, R. D. Effect of viscosity on drop breakup. *Int. J. Multiphase Flow* **20**, 211–216 (1994).

[13] Popinet, Stéphane Gerris: a tree-based adaptive solver for the incompressible Euler equations in complex geometries. *J Comput Phys* **190**, 572–600 (2003).

[14] Popinet, Stéphane An accurate adaptive solver for surface-tension-driven interfacial flows. *J Comput Phys* **228**, 5838–5866 (2009).

[15] Fuster, D. et al. Simulation of primary atomization with an octree adaptive mesh refinement and VOF method. *Int. J. Multiphase Flow* **35**, 550–565 (2009).